JGR Solid Earth

RESEARCH ARTICLE
10.1029/2021JB022693

Is Alteration of Magnetite During Rock Weathering Climate-Dependent?

Qi Zhang[1,2], Erwin Appel[2], Nathani Basavaiah[3], Shouyun Hu[4], Xiuhua Zhu[5], and Udo Neumann[2]

[1]Center for Marine Magnetism (CM2), Department of Ocean Science and Engineering, Southern University of Science and Technology, Shenzhen, China, [2]Department of Geosciences, University of Tübingen, Tübingen, Germany, [3]Department of Physics, Krishnaveni Degree & PG College, PG Research & Development, Narasaraopet, Guntur, India, [4]State Key Laboratory of Lake Science and Environment, Nanjing Institute of Geography and Limnology, Chinese Academy of Sciences, Nanjing, China, [5]Center for Earth System Research and Sustainability, University of Hamburg, Hamburg, Germany

Key Points:

- Stronger alteration of magnetite during rock weathering in wetter climates is indicated, but is hidden by source rock heterogeneity
- At equal humidity, magnetite alteration can be stronger in colder climates, possibly favored by frost-induced micro-cracks
- Magnetic records in sediment archives will likely not show humidity-related magnetite alteration effects acquired during rock weathering

Supporting Information:

Supporting Information may be found in the online version of this article.

Correspondence to:

E. Appel,
erwin.appel@uni-tuebingen.de

Citation:

Zhang, Q., Appel, E., Basavaiah, N., Hu, S., Zhu, X., & Neumann, U. (2021). Is alteration of magnetite during rock weathering climate-dependent? *Journal of Geophysical Research: Solid Earth*, *126*, e2021JB022693. https://doi.org/10.1029/2021JB022693

Received 25 JUN 2021
Accepted 23 SEP 2021

Abstract

Magnetic records in sedimentary sequences are often used as paleoclimate proxies. Climate-specific alteration of magnetite during rock weathering in the catchment might contribute to proxy variations in sediment sinks. In an actualistic study, we investigated the effects of magnetite alteration using weathered pebble material on basaltic parent rock. We collected samples from the Deccan basalts (India) across a large difference of mean annual precipitation (MAP; ~800–3,200 mm), and also from the Emeishan basalts (SW-China) to compare alteration effects at similar MAP (~1,100 mm) but ~12°C–15°C lower mean annual temperature (MAT). We used rocks with lamellar magnetite-ilmenite texture to ensure the best possible uniform parent rock magnetic mineralogy. We separated the weathered material into five groups by grain size, assuming that alteration increases in finer pebbles. Only magnetic susceptibility (χ) shows a systematic change, with an increase that is weakly stronger for higher MAP. Consistent with a simplified model, the χ-increase may represent progressive maghemitization. For the Emeishan basalts, we found a significantly stronger degree of alteration, including loss of magnetite. We explain this effect, which is surprising regarding the clearly lower MAT, by frost-induced micro-cracks due to physical weathering that opens pathways for oxygen and humidity into particle interiors. Based on these findings, we conclude that climate-related alteration effects of magnetite during rock weathering are in most cases outweighed by parent rock heterogeneity, and magnetic proxy records in derived sediment archives are unlikely to record climate-related magnetite alteration acquired during rock weathering, at least for catchment with basalts.

Plain Language Summary

Magnetite is of primary importance for magnetic records in paleoclimate archives such as lake sediments. Source material for archives derives from bedrock weathering. Possible climate-dependent alteration of magnetite during rock weathering may be an important factor controlling proxy variations. Previous results from lacustrine sediments indicated a relationship with humidity conditions in the catchment. To rate how significant such weathering effects are for interpreting paleoclimate records, we performed an actualistic study of magnetite alteration in rock weathering in dependence of climatic conditions, in particular mean annual precipitation (MAP). Using basalts as a common rock type, we compared fresh rock and related weathered material at sites with different MAP and different mean annual temperature (MAT). The results show that alteration of magnetite is only slightly stronger in wetter climates, but surprisingly clearly stronger in colder climates at same MAP. The latter is possibly due to micro-cracks formed through freezing and thawing that opens pathways for moisture and oxygen into particle interiors. Overall, the results suggest that climate-dependent magnetite alteration during rock weathering in the catchment is unlikely a controlling factor of paleoclimate records. Rock magnetic variability of source rocks will mostly hide these effects.

1. Introduction

Magnetic mineral assemblages, their concentration, and magnetic domain state in archives such as marine and lake sediments, loess deposits, and paleosols provide valuable information on paleoclimate studies (Long et al., 2011; Maher & Hu, 2006; Schwertmann, 1985). Multiple processes cause variations of magnetic

properties, including dilution by non-magnetic fractions (Peck et al., 1994), diagenetic effects such as dissolution of magnetic phases (Negrini et al., 2000) and authigenic formation of magnetic minerals (Snowball et al., 2002), and processes in the catchment during erosion and transport (Eriksson & Sandgren, 1999; Lise-Pronovost et al., 2014). Alteration of magnetic minerals also affects the stability of remanent magnetizations in rocks (Irving, 1970). Basalts play an important role for both paleomagnetism and as source material for paleoclimate archives, and alteration of their ferrimagnetic components (magnetite and titanomagnetite) during weathering may critically depend on climate conditions.

The alteration process of magnetite (including titanomagnetite) under normal atmospheric conditions progresses from crystal surfaces into the particle interior, gradually altering magnetite toward maghemite by oxidation of Fe(II) to Fe(III), associated with the formation of lattice vacancies (O'Reilly, 1984; Readman & O'Reilly, 1972) and lattice shrinkage (Gorski & Scherer, 2010). This low-temperature oxidation (LTO), also called maghemitization, causes particle-internal heterogeneity and inhomogeneous stress distribution leading to increased magnetic hardness (Appel, 1987; Cui et al., 1994; Keller & Schmidbauer, 1999; Wang et al., 2006). Formation of shrinkage cracks that develop at higher degree of LTO (Petersen & Vali, 1987) allows moisture and oxygen to penetrate into the interior of particles, thereby enlarging the effective crystal surface exposed to alteration. Strongly maghemitized magnetite can finally transform into hematite (Sidhu, 1988; Torrent et al., 2006) or goethite (He & Traina, 2007).

Weathering of parent rock produces erodible material that serves as the primary source for palaeoclimate archives such as lake sediments (Demory et al., 2005) or loess deposits (Liu et al., 2004). Weathering intensifies with humidity and temperature, and both lithology of parent rock and climate affect magnetic properties during chemical weathering (Su et al., 2015). However, the dependence of weathering rates on climate is not fully understood, even for silicate minerals (Bastian et al., 2017; Edwards et al., 2017). Humidity in soil was suggested as a major driver of pedogenic magnetite alteration (Maxbauer et al., 2016), and different magnetic characteristics were found in soil material from dry and wet grasslands (P. Zhang et al., 2016). Variation of magnetic properties in lacustrine sediments northeast and southwest of the Tibetan Plateau (Herb et al., 2013; Hu et al., 2015) and on the Indian subcontinent (Basavaiah et al., 2015) were interpreted to be due to both humidity-induced LTO of magnetite and hematite formation in the catchment. Swaddle and Oltmann (1980) found that LTO of magnetite differs for dry and hydrothermal conditions which may support an effect of humidity. In a laboratory experiment exposing magnetite for one year at 70°C under different humidity conditions, relatively strong LTO was detected for extreme humidity, but the results also indicated that the degree of maghemitization is not linearly related to humidity (Q. Zhang et al., 2021).

At the current state of knowledge, the relationship between magnetite alteration and humidity is poorly understood. Whether inorganic weathering of rocks in the catchment contributes systematically to climate-related variation of magnetic parameters in sinks of erosion material is an open question. To investigate the climate sensitivity of magnetite alteration during rock weathering, we performed an actualistic study in different climate settings. Basalts were targeted as parent rock as they are rich in ferrimagnetic minerals and release strongly magnetic eroded material into the system through weathering. In this study, we took samples in areas with different mean annual precipitation (MAP), and also compared regions with equal MAP and different mean annual temperature (MAT).

2. Materials and Methods

2.1. Sampling and Sample Preparation

Criteria for selection of sampling sites were (a) a sufficiently uniform rock magnetic mineralogy in different climatic settings, and (b) a large ferrimagnetic content that allows studying representative small samples on a meaningful statistical level and to perform significant microscopy observations. We chose basalts from the Deccan Traps in India and from the Emeishan Traps in southwestern China. Basalts contain up to several percent of (titano-)magnetite, thus contributing the predominant magnetic source material for sedimentary sinks in these regions, similar to other areas on Earth where basalts occur in the catchment. The 500,000 km^2 large Deccan flood basalts (Figure 1a) erupted around the Cretaceous-Tertiary boundary (Allegre et al., 1999; Basavaiah et al., 2018). They stretch over a large gradient of MAP from ~800 to ~3,200 mm (Figure 1c), with high MAT of ~24°C–27°C (climate-data.org). About 80% of rainfall occurs

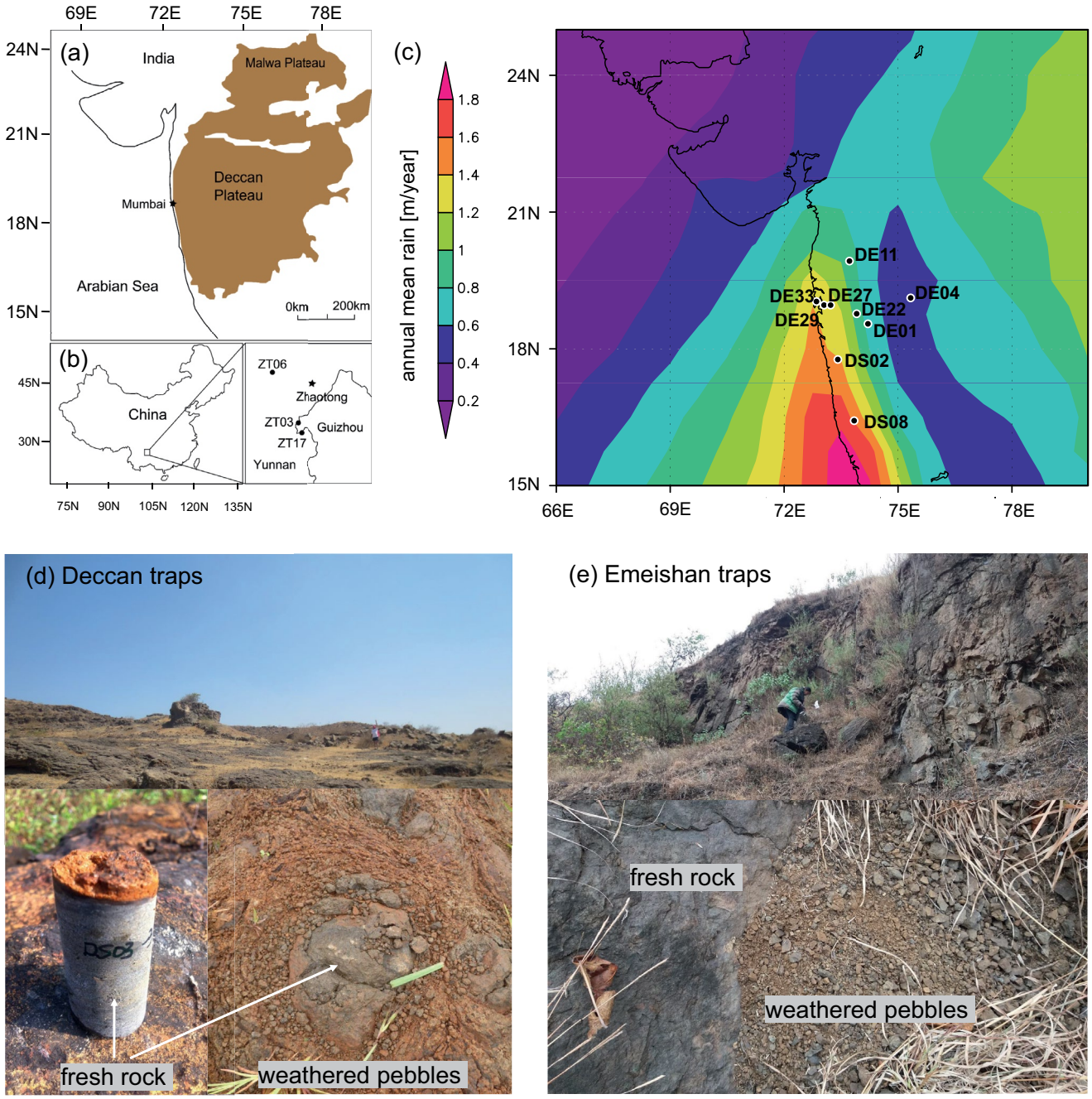

Figure 1. (a) Geology map of the Deccan traps in India, modified from Sheth (2005) and (b) sampling sites ($N = 3$) in the Emeishan traps, SW-China. (c) Mean annual precipitation map (ERA-Interim reanalysis of 35-year climate averages after Dee et al. [2011]) of India with sampling sites ($N = 9$) in the Deccan traps; the reanalysis data show the modeled trend of decreasing MAP from coastal areas to the inland, and increasing MAP in coastal areas from north to south in the sampling region. (d, e) Photographs of typical sampling sites: (top) outcrop settings, (bottom) drilled fresh rock sample, and close views of sampling spots that show how pebbles are related to the fresh rock.

during the monsoon season. The Deccan lavas are predominantly tholeiitic with a wide variety in the textural character (Wensink, 1973). Most of the extensive previous magnetic research on the Deccan Traps focused on paleomagnetism. Investigations of rock magnetic properties suggest a variety in domain structure and composition of the (titano-)magnetites (Radhakrishnamurty & Sahasrabudhe, 1967; Radhakrishnamurty et al., 1977), and in the degree of maghemitization (Radhakrishnamurty et al., 1978). The Permian Emeishan Traps (Figure 1b) in southwest China cover an area of ~0.3×10^6 km^2 (Shellnutt & Jahn, 2011).

They are flood basalts as the Deccan Traps, and geochemical data indicate both high-Ti and low-Ti lavas (Xu et al., 2001). MAP and MAT in the sampling area of the Emeishan Traps are ~1,100 mm and ~12°C, respectively (climate-data.org).

At each site, we sampled fresh (apparently non-weathered) parent rock and related pebbles on the rock surface. We chose spots where the pebbles could be clearly identified as a weathering product of the underlying rock (Figures 1d and 1e). In a first field campaign in 2015, we collected samples from 42 locations in the Deccan Traps distributed across the MAP gradient, and from 17 locations in the Emeishan Traps. We tested these samples for their rock magnetic mineralogy, in particular, searching for sites with magnetite as the only ferrimagnetic mineral. Nine sites from the Deccan Traps and three sites from the Emeishan Traps (Figures 1b and 1c and Table 1) were chosen, based on thermomagnetic curves and microscopic observations (Figure 2; see Section 2.3). In 2017, we then sampled the selected 12 sites in more detail. We collected fresh rock (drilled samples and samples crushed by hammer) and pebbles (~100 g at each spot) from five different spots at each site distributed across an area of maximum ~10^2–10^3 m^2, choosing barren spots to avoid an influence of pedogenesis. The pebble samples were sieved and divided into five sub-sample fractions by grain size (WP1 > 4 mm, WP2 2–4 mm, WP3 1–2 mm, WP4 0.5–1 mm, WP5 < 0.5 mm), assuming a tendency of stronger weathering with fining of the pebbles. For bulk magnetic measurements, the major part of the sample materials was placed into cylindrical plastic boxes and weighed, and the retained material was used for thermomagnetic measurements and microscopy.

2.2. Analytical Methods

We measured room temperature magnetic susceptibility (χ) at frequencies of 976 and 15,616 Hz (χ_{lf} and χ_{hf}) on an MFK-1 Kappabridge (Agico), recording the results as mass-specific values. From the χ-results, we calculated the frequency-dependence of χ (χ_{fd}%) by $[(\chi_{lf}-\chi_{hf})/\chi_{lf}] \times 100$ (Dearing et al., 1996). Using a KLY-3 Kappabridge (Agico) combined with a CS-3 furnace and a CS-L cryostat, we performed high-temperature (room temperature to 700°C in air) and low-temperature (−196°C to room temperature) thermomagnetic runs of magnetic susceptibility (χ-T curves). Two remanence parameters, isothermal remanent magnetization (IRM) and anhysteretic remanent magnetization (ARM) were measured. We obtained ARMs using a DC-SQUID magnetometer (2G Enterprises) with attached degausser (decaying alternating field of max. 100 mT) and DC field coil (superimposing a 50 μT DC field), and IRMs using an MMPM9 pulse magnetizer and a Molspin spinner magnetometer. The IRM imparted at 2 T was considered as saturation IRM ($SIRM_{2T}$), and an S-ratio was calculated from $SIRM_{2T}$ and an IRM acquired at a reverse field of 300 mT ($IRM_{-0.3T}$) by $[1\text{-}IRM_{-0.3T}/SIRM_{2T}]/2$ (Bloemendal et al., 1992). Moreover, we measured first-order reversal curves (FORCs) on an 8600 Series VSM (Lake Shore Cryotronics) at room temperature and a maximum field of 1 T, using samples of ~1 g, and processed the curves with software FORCinel (Harrison & Feinberg, 2008).

We examined polished sections (obtained by final polishing with diamond paste of 1 μm grain size) of fresh rocks and pebbles from each sampling location by reflected light microscopy, using immersion oil for higher resolution, and applying ferrofluid for clear identification of strong magnetic phases. Moreover, we performed scanning electron microscopy (SEM) using an LEO 1450VP microscope with tungsten filament, operated at 15-kV acceleration voltage, and equipped with an energy-dispersive x-ray spectroscopy (EDX) detector.

FORCs were measured at the Center for Marine Magnetism (CM2), Southern University of Science and Technology, other analytical work was carried out at the Department of Geoscience, University of Tübingen.

The used values of climate parameters are reanalysis model data from climate-data.org and from ERA5 (Hersbach et al., 2020) (Table 1). MAP and MAT are skin data (values at surface), and mean annual specific humidity (Q) refers to 1,000 hPa. In climate-data.org values for specific cities/towns are given. For the Deccan sites, the maximum distance of the sampling site to the chosen place in climate-data.org is ~10 km; for the Emeishan sites, the distance is 30–35 km. ERA5 provides single grid-cell data (spatial resolution 0.28125°), and after accumulating or averaging daily data for the period 1990–2019, we used the results from the grid-cell in which the respective sampling site is located. The considered period of climate-data.org data is 1999–2019, the underlying spatial resolution is 0.1–0.25°, how the data were processed (smoothing, etc.) is not stated by the data source.

Journal of Geophysical Research: Solid Earth

10.1029/2021JB022693

Table 1
Climate Parameters, and Mean Values (With Standard Deviations) of Magnetic Results of the 12 Studied Sites

Site name	Latitude/ longitude	Elev.	Place name	MAP	MAT	MAP	MAT	Mean Q	χ	SIRM	S-ratio	χ_{fd}	SIRM/χ	ARM/SIRM
	°N/°E	[m]		[mm]	[°C]	[mm]	[°C]	[g/kg]	[10^{-8} m^3/kg]	[Am^2/kg]	[–]	[%]	[kA/m]	[–]
			climate-data.org				ERA5							
Deccan basalts														
DE01	18.4158/74.0053	843	Sasvad	778	23.5	761	24.5	12.0	1,402.6 ± 492.8	0.44 ± 0.24	0.99 ± 0.009	3.34 ± 1.67	30.57 ± 9.08	0.0043 ± 0.0009
DE04	19.0951/74.8361	816	Bhingar	836	24.8	785	28.6	11.3	340.6 ± 102.8	0.08 ± 0.03	0.94 ± 0.025	8.13 ± 3.4	23.13 ± 6.25	0.0065 ± 0.0018
DE11	19.9383/73.5255	755	Khambale	925	26.3	2,274*	25.8	12.8	455.9 ± 170.9	0.08 ± 0.03	0.97 ± 0.017	4.96 ± 2.82	16.78 ± 1.56	0.0054 ± 0.0013
DE22	18.6812/73.7234	624	Talegaon-Dabhade	1,093	24.0	1,186	23.7	12.4	632.9 ± 155.2	0.17 ± 0.03	0.98 ± 0.005	3.33 ± 1.42	27.01 ± 6.44	0.0043 ± 0.0025
DE27	18.9097/73.2100	39	Matheran	1,750	25.9	1,754	26.8	14.5	852.5 ± 227.5	0.21 ± 0.02	0.98 ± 0.009	2.7 ± 0.54	26.91 ± 11.39	0.0049 ± 0.0018
DE29	18.9732/73.0333	5	Navi- Mumbai	1,915	26.6	1,754	26.8	14.5	602.3 ± 127.3	0.09 ± 0.02	0.95 ± 0.020	9.74 ± 2.12	14.92 ± 1.96	0.0097 ± 0.0007
DE33	19.1403/72.9173	71	Mumbai	2,012	26.4	1,751	27.0	15.3	2,358.3 ± 187.0	0.08 ± 0.02	0.99 ± 0.003	2.58 ± 0.14	3.43 ± 1.10	0.0104 ± 0.0012
DS08	16.5443/73.6316	33	Kharepatan	2,983	26.1	3,106	26.8	14.6	2,525.9 ± 120.6	0.38 ± 0.06	0.99 ± 0.004	3.76 ± 0.22	14.89 ± 2.70	0.0056 ± 0.0010
DS02	17.6969/73.4084	36	Khed	3,232	25.9	3,382	26.7	14.6	1,543.9 ± 192.6	0.23 ± 0.03	0.99 ± 0.007	3.98 ± 0.72	14.71 ± 0.75	0.0082 ± 0.0005
Emeishan basalts														
ZT03	27.0763/103.6465	1,848	Zhaotong	1,098	11.8	1,383	12.1	8.4	1,282.9 ± 337.8	0.34 ± 0.07	0.99 ± 0.008	3.19 ± 0.07	26.99 ± 3.63	0.0053 ± 0.0006
ZT06	27.4061/103.4229	2,189	Zhaotong	1,098	11.8	1,179	12.7	8.3	2,483.8 ± 431.3	0.31 ± 0.11	0.99 ± 0.004	2.70 ± 0.18	12.73 ± 4.44	0.0050 ± 0.0015
ZT17	27.0255/103.6471	1,542	Zhaotong	1,098	11.8	1,383	12.1	8.4	1,232.6 ± 225.6	0.25 ± 0.04	0.99 ± 0.008	3.14 ± 0.27	20.32 ± 4.62	0.0060 ± 0.0008

Note. GPS coordinates and elevations (elev.) of the studied sites. Climate parameters (MAP and MAT: mean annual precipitation and temperature at surface; Q: mean annual specific humidity at 1,000 hPa) are reanalysis model data from climate-data.org and from ERA5; places from which climate-data.org were taken are listed (maximum ~10 km distance from the respective site for Deccan basalts, 30–35 km distance for Emeishan sites); the high MAP-value of site DE11 (marked by *) from ERA5 is probably due to extreme local rainfall events. Magnetic data are mean values and standard deviations of the five sub-samples from pebble fraction WP1, for χ (magnetic susceptibility), χ_{fd}% (percentage frequency-dependent susceptibility), SIRM (saturation isothermal remanent magnetization), S-ratio and ratios of SIRM/χ and ARM/SIRM (ARM: anhysteretic remanent magnetization). WP1 data are used for normalization of FR and WP data (Table S2).

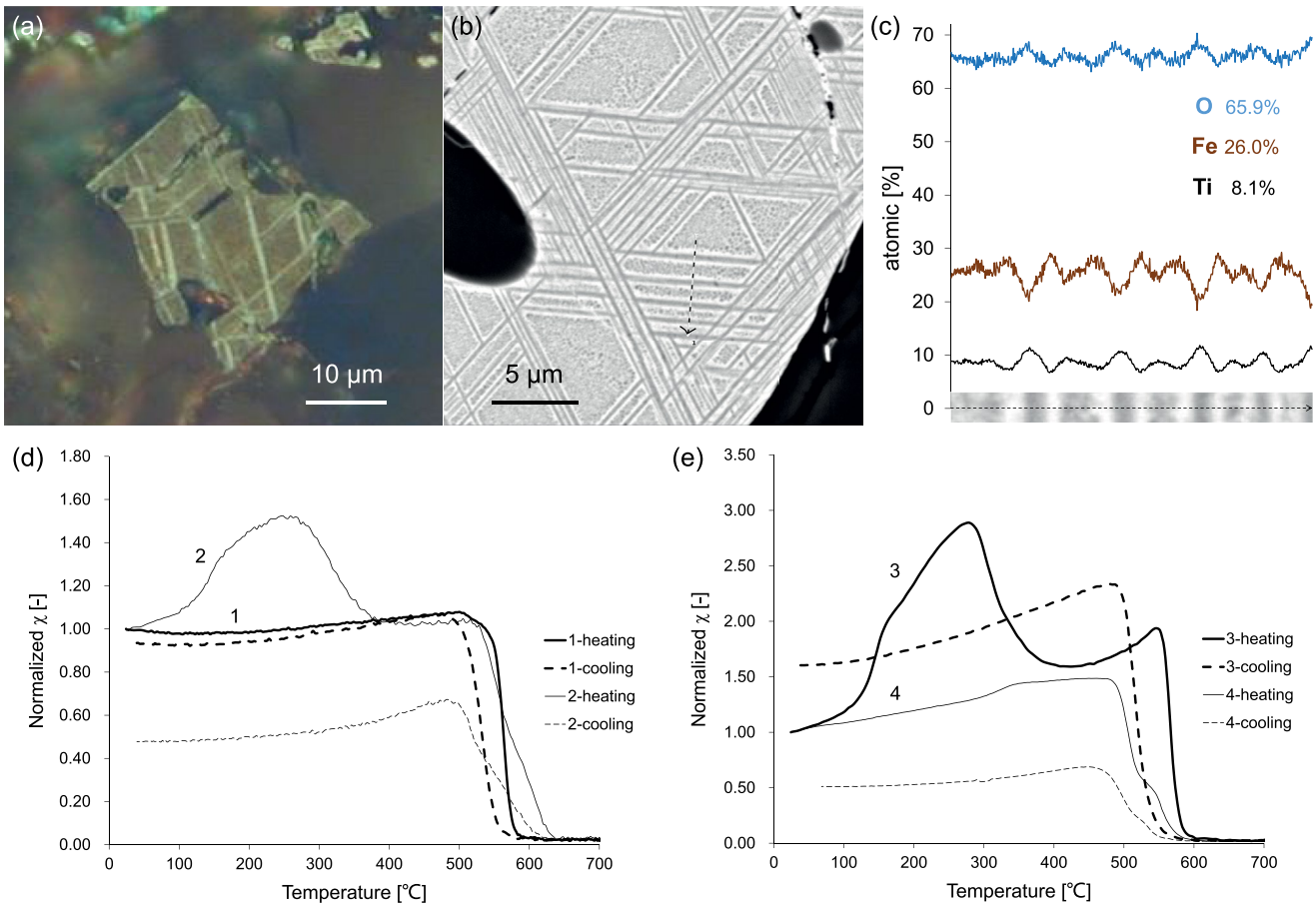

Figure 2. (a, b) Lamellar structures of magnetite (with possibly minor Ti-substitution) and non-ferrimagnetic ilmenite. Magnetite is identified in the optical micrograph (a) by coverage with ferrofluid nanoparticles (dark color), while non-ferrimagnetic phases (light color) do not attract ferrofluid particles; the reflectivity contrast in the SEM image (b) discriminates the two phases (dark color represents magnetite); EDX analysis (c) shows different Fe and Ti contents on a line scan (along the dashed line in b) across the dark/light contrast (the EDX result integrates on both phases as the lamellar structure is finer than the analyzed spot size; the inclined electron beam causes a shift between the scanned dark-light SEM stripe at the bottom and the EDX results). (d, e) Typical thermomagnetic (χ-T) curves of fresh rock samples from sites accepted (d) and rejected (e) for this study: (d) curves indicating magnetite as single ferrimagnetic phase (curve 1), with partly fine particle behavior indicated by the hump-like shape (curve 2); (e) curves indicating Ti-rich titanomagnetite that forms magnetite at higher temperature (curve 3), or representing coexisting magnetite and Ti-poor titanomagnetite (curve 4).

2.3. Site Selection

We rejected sites (a) with evidence of Ti-rich titanomagnetite and (b) coexistence of magnetite and Ti-poor titanomagnetite. Preferred sites contain coexisting magnetite and ilmenite (Figures 2a–2c), formed by exsolution of Ti-rich titanomagnetite into trellis-type lamellar textures of magnetite (or Ti-poor titanomagnetite) and ilmenite (Ramdohr, 1980) during relatively slow cooling. This type of magnetic mineralogy is a primary feature of the original genesis of the basalts (Mücke, 2003; Su et al., 2015). Strongly magnetic phases could be clearly identified by optical microscopy through coverage with ferrofluid (Figure 2a). Because of irregular surface stress due to mechanical polishing, the magnetite fractions typically show a complex ferrofluid pattern (so-called maze pattern; Bozorth, 1951).

High-temperature χ-T curves provided the best method for selecting appropriate samples. Samples only containing magnetite as a ferrimagnetic phase show approximately constant χ (determined by the inverse of the demagnetization factor) between room temperature and close to the Curie temperature (T_c) of around 580 °C (no. 1 in Figure 2d). Presence of Ti-rich titanomagnetite that may be preserved by fast cooling is typically indicated by skeletal-shaped particles (Mollo et al., 2013), an additional intermediate T_c in the χ-T curves (Figure 2e), increasing χ before T_c (Appel & Soffel, 1985), and transformation into magnetite at higher temperature associated with strongly increasing χ in the χ-T runs (no. 3 in Figure 2e). Sites with such

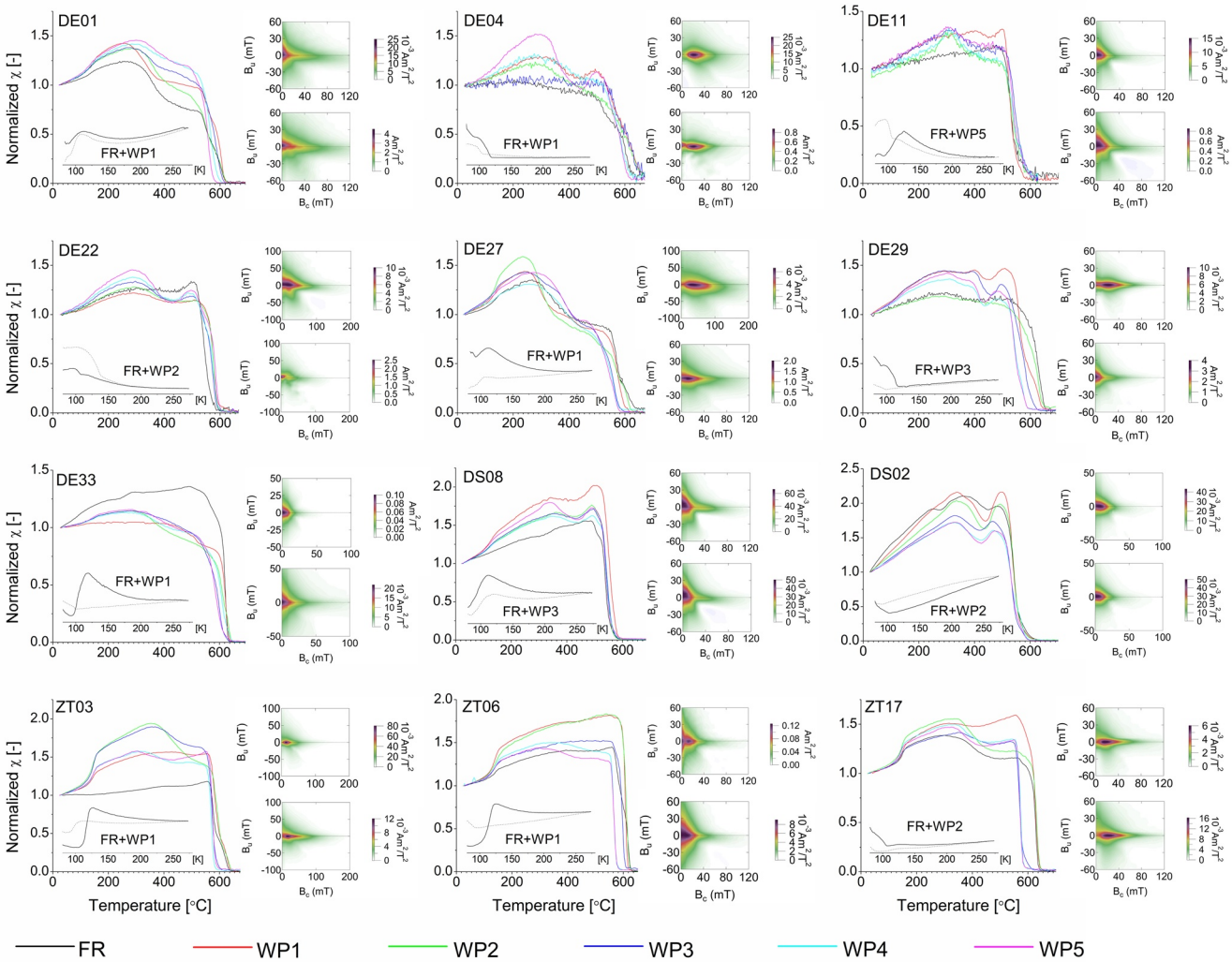

Figure 3. High and low-temperature thermomagnetic curves (χ-T) of fresh rock (FR) and weathered pebbles (WP) from all sites (WP1 > 4 mm, WP2 2–4 mm, WP3 1–2 mm, WP4 0.5–1 mm, WP5 < 0.5 mm). Only heating curves are shown for high-temperature thermomagnetic curves. Solid and dashed lines of low-temperature thermomagnetic curves represent fresh rock and weathered pebble (WP fraction labeled) samples, respectively. To the right of the χ-T plots, FORC diagrams (smoothing factor 4) of FR (top) and WP2 (bottom) are shown.

indications for Ti-rich titanomagnetite were rejected. We also excluded sites for which χ-T curve revealed magnetite and a Ti-poor titanomagnetite with clearly distinguishable T_c close to magnetite (no. 4 in Figure 2e). A hump-like shape at intermediate temperature was often observed in χ-T curves during heating, with no indication for transformation into magnetite (no. 2 in Figure 2d). As we will further discuss in Section 4.4, the hump is most likely caused by transition from stable single-domain (SSD) to the superparamagnetic (SP) state, and the width of the hump reflects different SSD-SP transition temperatures due to a range of magnetic grain sizes (Q. Zhang et al., 2021). Sites with such χ-T curves we also classified as sites with exclusive magnetite as a ferrimagnetic fraction.

3. Results

Figure 3 shows representative high-temperature χ-T curves of fresh basalts and weathered pebbles from each of the 12 selected sites (for clearness only heating curves are shown). Values of T_c estimated from heating curves range from ~580 to ~660°C. These T_c values might overestimate the true T_c by up to ~15°C, as due to different heat capacities the thermoelement adjusts faster to temperature changes than the sample (causing a thermal hysteresis of up to ~30°C between heating and cooling curves). Most samples reveal a

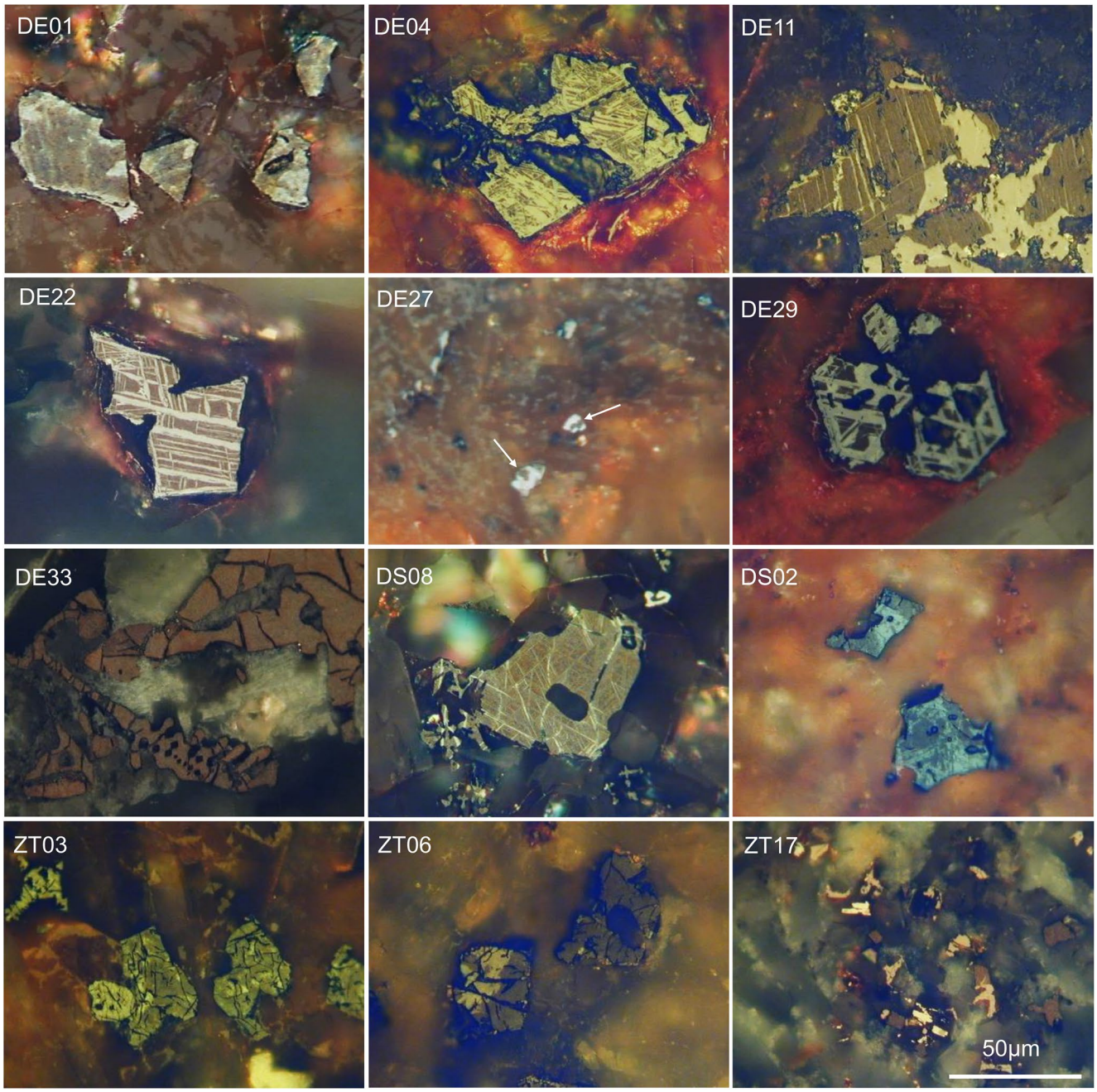

Figure 4. Optical micrographs of basalt samples from each study site, with application of ferrofluid for identifying strong magnetic phases (dark areas on oxide grains). Different brightness and color are due to the concentration of the ferrofluid. The two arrows in the DE27 image point to small grains where ferrofluid coverage is visible on part of the grains.

hump-like peak at around 300°C–350°C. Some sites show a more pronounced hump with decreasing particle size, which is most systematic for DE22. Moreover, we observed less significant changes between heating and cooling curves for fresh rock than for pebbles fractions. Only a few low-temperature thermomagnetic curves display a Verwey transition (Figure 3). It is known that the Verwey transition is very sensitive to the degree of maghemitization and disappears at ~15% of maximum oxidation (Aragón et al., 1985), thus the absence of the transition does not exclude the (sole) presence of maghemitized magnetite.

Optical micrographs of polished sections of all 12 selected sites are shown in Figure 4. Ten sites are dominated by large magnetite-bearing grains of several tens of microns (DE01, DE04, DE11, DE22, DE29, DE33,

DS02, DS08, ZT03, and ZT06), while two sites contain only small grains of few microns in size (DE27 and ZT17). Lamellar magnetite-ilmenite intergrowth is clearly revealed within the larger grains for most sites, but also entirely ferrofluid-covered particles exist in some cases (e.g., DE33). However, exsolutions may also exist in the latter, with finer texture below optical resolution. The observed differences in size and texture are probably due to variable types of magma sources and different cooling rates of the basalts.

For analyzing bulk magnetic data (for raw data see Table S1), we first normalized all values from the same sub-sampling spot by the mean value of the corresponding WP1 (Table 1). We then applied linear regression analyses for each site using all sub-sample results as individual data of equal weight (i.e., maximum 30 data points per site), and recorded the regression result by the slope value (with its 95% confidence interval) for the assumed sequence of the weathering degree. The abscissa values were set as 0–5 for FR-WP1-WP2-WP3-WP4-WP5. We performed the regression analysis for four different sub-sample sets: (a) fresh rock and weathered pebbles WP1-5, (b) weathered pebbles WP1-5, (c) fresh rock and weathered pebbles WP1-4, and (d) weathered pebbles WP1-4. For significantly variable magnetic properties of the parent rock at different spots, a substantial source of error might arise from non-detected lateral displacement of the pebble material from its true origin in the parent rock. If the pebble sample is contaminated by material affected by pedogenesis, the latter will predominantly influence the results of the finest pebble fraction (WP5). Pedogenic influence and uncertainty in the spatial relation of the pebbles and the FR sample is best avoided by including only the pebble fractions WP1–WP4 in the analysis, and this will also ensure that all samples are exactly from the same spot.

All four different variants of grouping yield very similar results (Table S2). Figures 5 and 6 show the slope results of one magnetic concentration parameter (χ) and one parameter ratio (SIRM/χ) sensitive to domain-state and magnetic mineral composition, respectively (including FR and all WP fractions). Slope results for other parameters (SIRM, S-ratio, χ_{fd}%, ARM/SIRM) are shown in Figures S1–S4.

The Deccan sites show a complex pattern with increasing and decreasing slope values for same parameters. S-ratios are generally close to the theoretical maximum (1.0) and thus do not provide discriminative information. Frequency-dependent susceptibility (χ_{fd}%) values are small and similar in most sites (~2%–5%), being higher only for DE04 and DE29 (~8%–9%). The trend of χ_{fd}% values with decreasing pebble size is mixed, and these results are not meaningful bearing in mind the relatively small degree of changes and the accuracy of the data.

The behavior of magnetic parameters and ratios of the Emeishan basalts is more consistent than for the Deccan basalts. With fining of the pebbles, the concentration-dependent parameters χ and the SIRM both reveal a decrease trend, the SIRM/χ ratio clearly decreases (ZT03 only within confidence limits), the ARM/SIRM ratio shows a trend toward higher values, and χ_{fd}% also seems to increase (though not significantly with respect to confidence limits).

FORC diagrams (Figure 3) of fresh rock and weathered pebbles (WP2) reveal different characteristics for the studied sites, showing SSD and SP properties with variable degree of magnetic interaction, as well as multidomain (MD) behavior (Roberts et al., 2014). No systematic differences of these characteristics can be recognized between FR and WP samples.

4. Discussion

4.1. Response of Magnetic Parameters to Magnetite Alteration

Numerical slope results of linear regression are consistent for the different data groupings (Table S2 and Figures S5–S10). Possible uncertainty in the relationship of the pebbles (WP) to their fresh rock sample (FR) and pedogenic influences is therefore not relevant. For further discussion, we use the results from the FR and WP1–4 grouping (data 0–4 in Table S2). WP5 data are excluded because these are not available for DE01 and DE27. Additionally, as an alternative measure of weathering changes, we calculated the ratio of the WP2 (2–4 mm fraction) and FR values (Table S3). WP2 was taken because larger pebbles best avoid possible contamination by pedogenic material, and WP2 has a more uniform size distribution for the 12 sites than the largest pebble fraction (WP1). Slope and WP2/FR results for χ, SIRM, SIRM/χ, and ARM/SIRM are

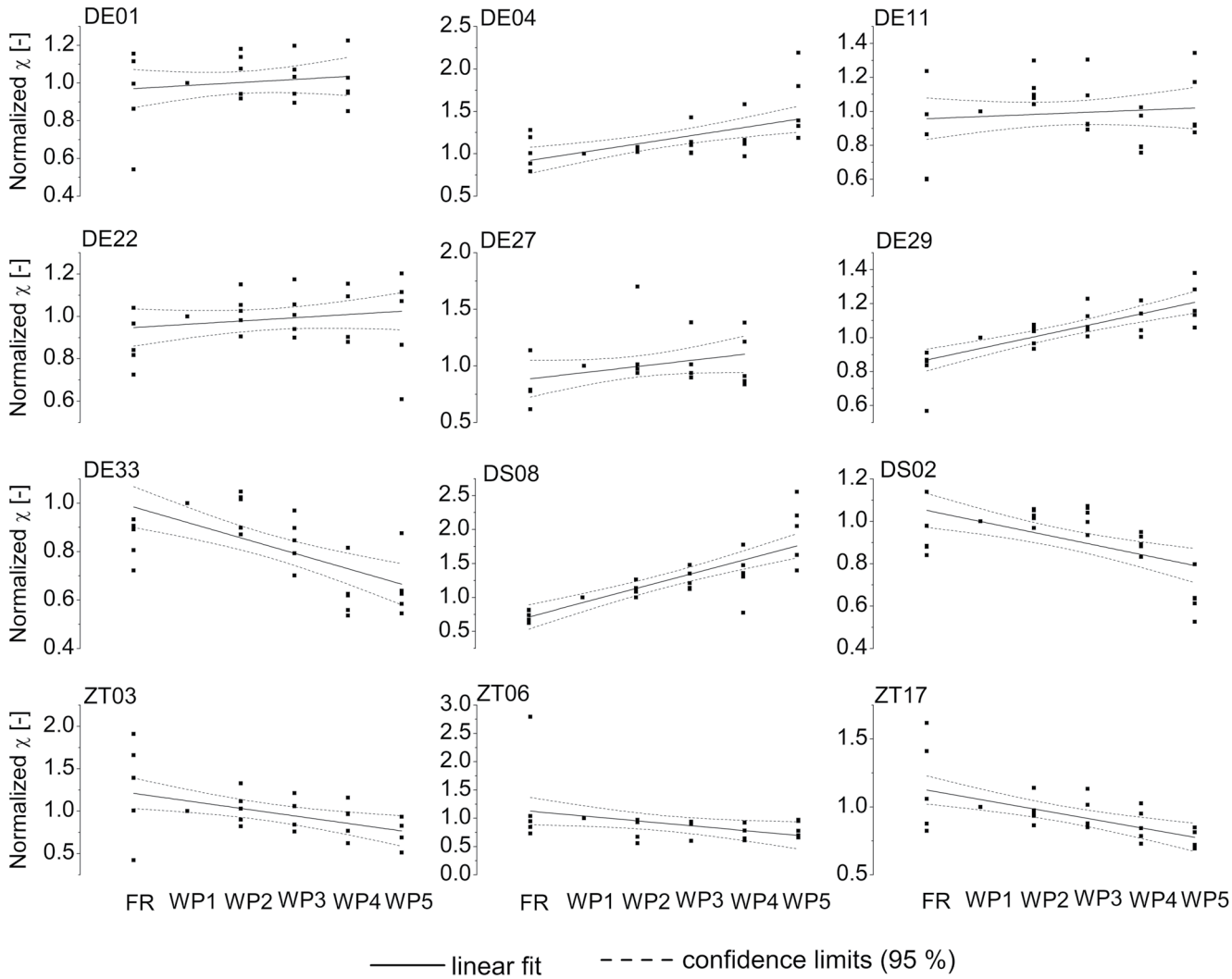

Figure 5. Magnetic susceptibility (χ) versus alteration degree (assumed to increase from FR to WP5), all values normalized to WP1 of each sub-sample set. Linear fits with 95% confidence intervals are shown; due to lack of material, there are no WP5 data for DE01 and DE27.

largely consistent (Figure S11), with few deviations (DE04, DE11, and DE33) and one outlier (SIRM/χ of DE33, which is due to deviation of SIRM and χ into opposite directions).

Magnetite alteration includes two processes, progressive maghemitization (Özdemir & Dunlop, 2010) and transformation into hematite (and finally into goethite as the last weathering product) (Abrajevitch & Kodama., 2009). Which response of magnetic parameters and ratios do we expect due to alteration? Concentration-dependent parameters (χ, SIRM, ARM) will generally decrease when magnetite is lost (no matter if it is stoichiometric or maghemitized). However, these parameters might also change by a shift of the effective magnetic grain size (i.e., magnetic domain state) (Figure 7a). Figures 7c–7e show bivariate plots of parameter changes WP2/FR for the Deccan and Emeishan sites. S-ratio values close to 1 for nearly all samples (Table S1) imply that the ARM/SIRM ratio is dominated by magnetite. The ARM/SIRM ratio is higher in SSD grains compared to larger grains (Yamazaki & Ioka, 1997). We assume that spin rotation-controlled magnetization processes (in SSD grains and in particles with internal sub-division) increase the ARM/SIRM ratio. A decrease in physical grain size might be caused by the partial transformation of magnetite into hematite, and more intense particle-internal sub-division is expected by progressing maghemitization that decreases the effective magnetic grain size through heterogeneous internal stress distribution (Appel, 1987).

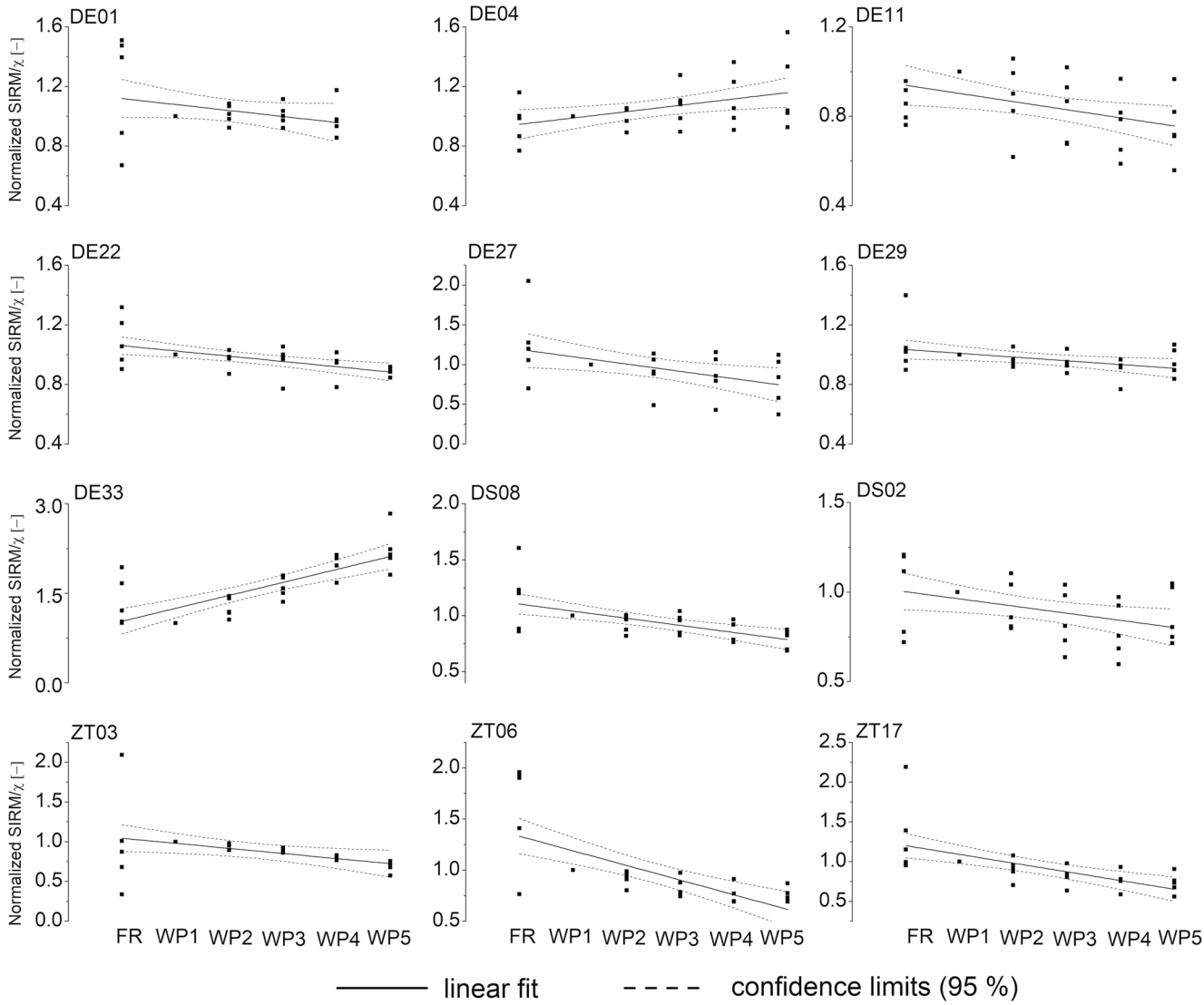

Figure 6. SIRM/χ ratio (ratio of saturation isothermal remanence and magnetic susceptibility) versus alteration degree (assumed to increase from FR to WP5), all values normalized to WP1 of each sub-sample set; due to lack of material, there are no WP5 data for DE01 and DE27.

We modeled the effect of (inhomogeneous) maghemitization by a shift of an initial magnetic grain size distribution (D-0 in Figure 7b) toward a distribution with finer particle behavior (D-1 in Figure 7b). In a second model, we reduced the D-1 distribution linearly by a certain factor that simulates a 40% loss of magnetite (D-2 distribution in Figure 7b). The assumed simplified parameter dependences of χ, SIRM and ARM are shown in Figure 7a. We took a constant χ-value in the SSD and MD range, and an up to 2.5 times increase of χ in the SP range. The chosen χ-enhancement in the SP range is relatively moderate compared to theoretical predictions (Kodama, 2013; Worm, 1998). The constant χ-value corresponds to the inverse of the demagnetization factor (N) due to high intrinsic susceptibility χ_i ($N\chi_i >> 1$). Slightly smaller χ-values for SSD compared to MD magnetite (Maher, 1988) are of subordinate relevance for the principal modeling results. For the relative difference of ARM and SIRM in the SSD and MD range, we approximately followed the results of Maher (1988) and Dunlop (2002), and we assumed that ARM is inversely proportional to the particle diameter in the fine pseudo-SD (PSD) range (Dunlop & Argyle, 1997). Occurrence of magnetite in fine exsolution structures as observed in the studied basalts favors domain states in the PSD-SSD-SP range. Because of additional internal sub-division due to inhomogeneous stress (as expected in altered magnetite), domain wall movement-controlled "true" MD behavior is likely of subordinate importance.

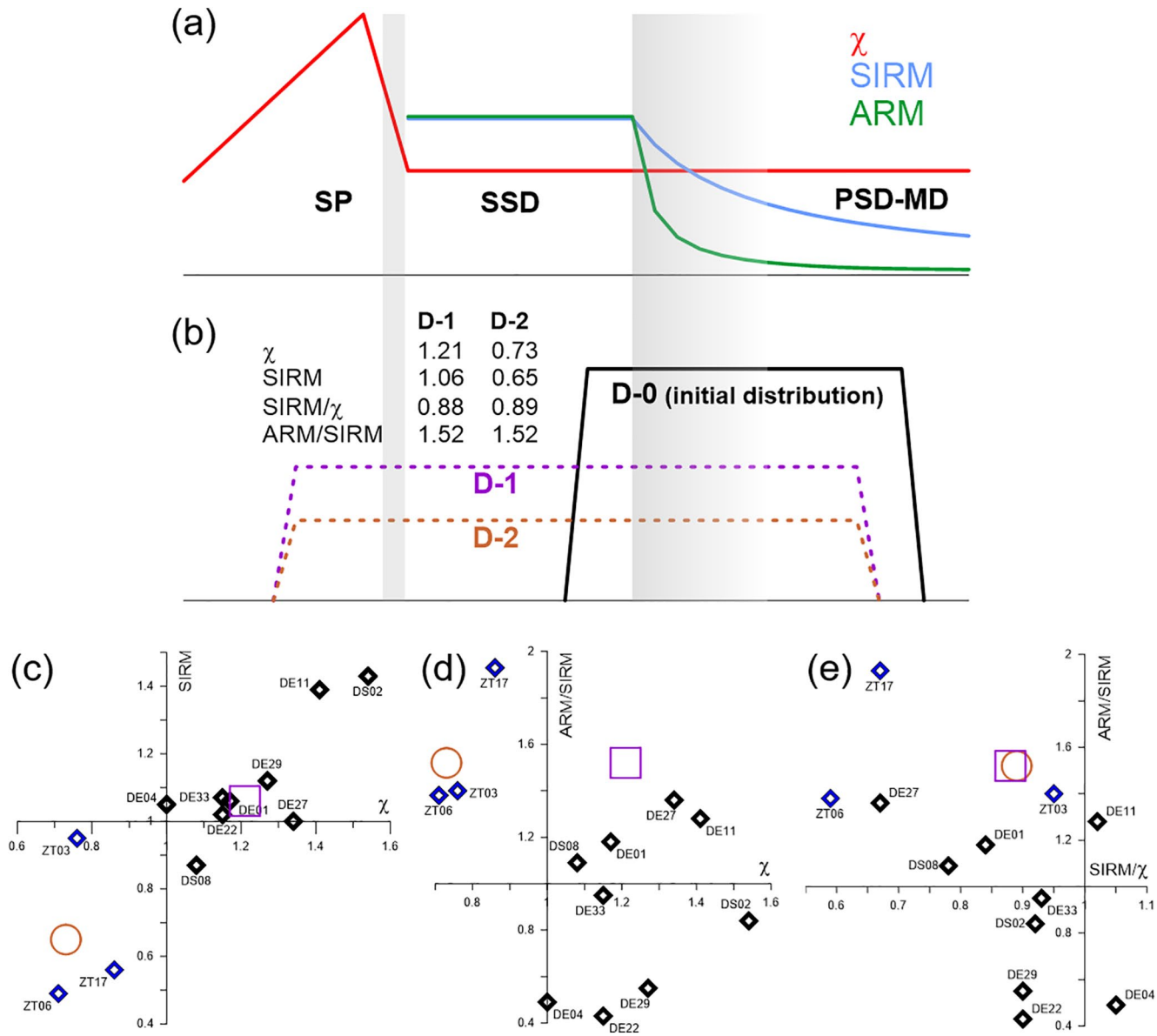

Figure 7. (a) Relative variations of magnetic parameters (χ, SIRM, ARM) versus grain size (i.e., magnetic domain state) used for modeling changes of χ, SIRM, SIRM/χ, and ARM/SIRM. (b) Magnetic grain size distributions of magnetite (D) as input for modeling: D-0 initial distribution, D-1 resulting from a shift toward fining of magnetic grain size (as due to inhomogeneous maghemitization), and D-2 additionally including transformation of 40% magnetite to hematite. The gray vertical bars indicate the SP-SSD and SSD-MD transitions; the left end of the gray SSD-MD range represents the theoretical transition, but magnetization by spin rotation processes extend into the MD region contributing to PSD properties (SP: superparamagnetic, SSD: stable single domain; PSD: pseudo-single domain, MD: multidomain). (c)–(e) Bivariate plots (χ vs. SIRM/χ, ARM/SIRM vs. χ, ARM/SIRM vs. SIRM/χ of WP2/FR means for the Deccan and Emeishan sites (data in Table S3); positive axes represent increased values of WP2 compared to FR; modeled results of D-1/D-0 and D-2/D-0 are shown in these plots by purple squares and brown circles, respectively (in the model, new hematite formed on expensive of magnetite is considered with a 98% remanence intensity reduction for SIRM and ARM).

The shift from D-0 to D-1 (reflecting maghemitization without transformation of the maghemitized spinel structure) causes an increase of χ (due to the shift into the SP range) and also a slight increase of SIRM (increased SSD fraction counterbalancing the shift into the SP range), which is in accordance to the measured data from the Deccan basalts (Figure 7c). Additional loss of magnetite (D-2) drives both χ and SIRM to values < 1.0 (i.e., decreasing values compared to D-0), which matches with observed results for the Emeishan basalts (Figure 7c). The model results explain the observed decrease of the SIRM/χ ratio for both groups of basalts (Figure 7e), and also the increase of the ARM/SIRM ratio for the Emeishan basalts. The

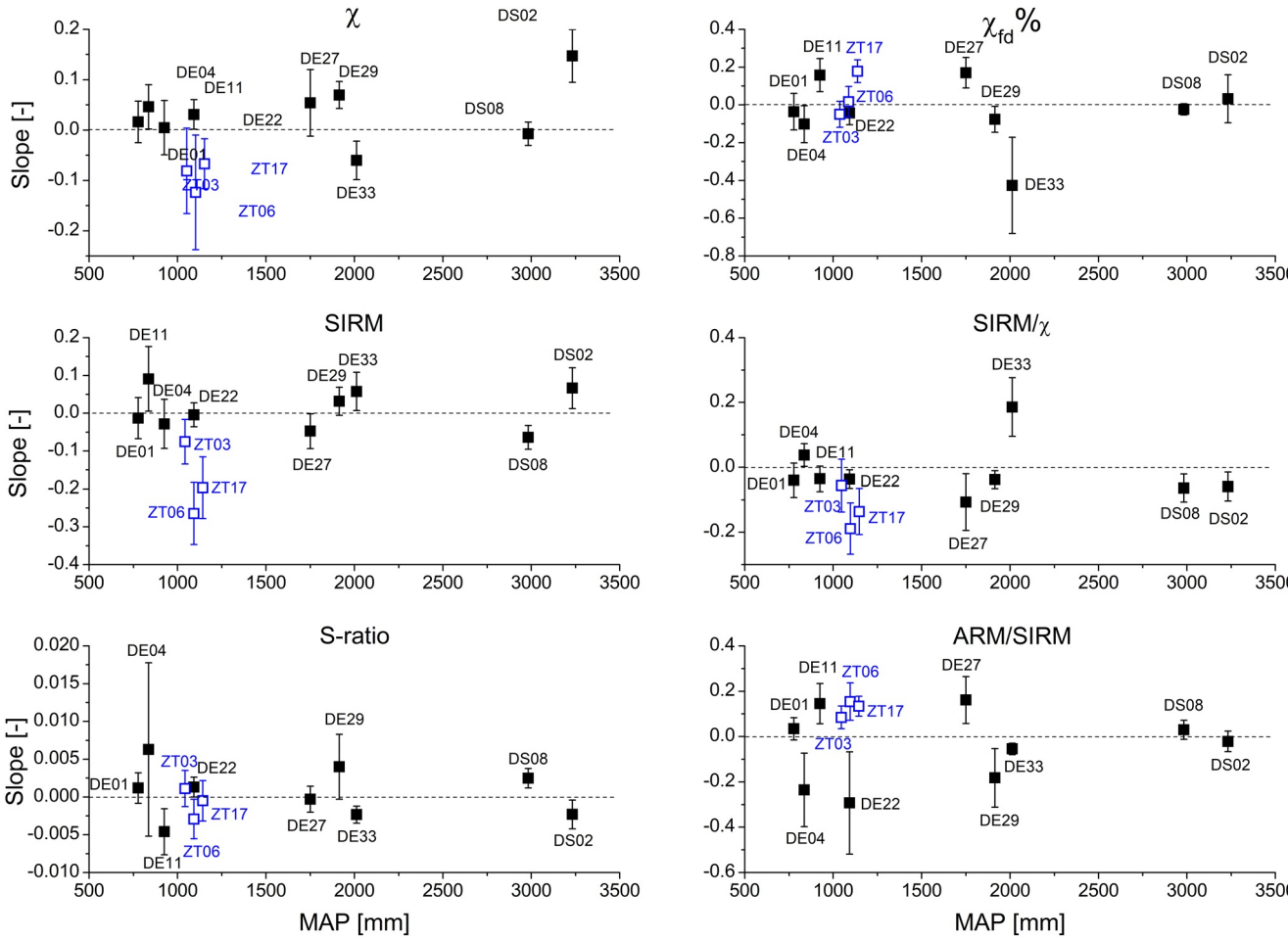

Figure 8. Slope values of regression lines including pebble fractions 1–4 (WP1-4) (see Table S1 for numerical results) versus mean annual precipitation (MAP) from climate-data.org, with 95% confidence limits, for χ (magnetic susceptibility), χ_{fd}% (percentage frequency-dependent susceptibility), SIRM (saturation isothermal remanent magnetization), S-ratio and ratios of SIRM/χ and ARM/SIRM (ARM: anhysteretic remanent magnetization). Black and blue symbols denote Deccan and Emeishan results, respectively. For plotting, MAP-values of ZT03 and ZT17 are shifted by −50 and +50 mm, respectively, to avoid overlapping.

decrease of the ARM/SIRM ratio that appears in part of the WP fractions of the Deccan basalts cannot be validated by the models, possibly because of the simplified assumed mechanism of ARM acquisition. Loss of part of the D-0 distribution at its left end (i.e., the fraction with finer particle behavior), by transformation into a low-magnetic or non-magnetic phase, would lower the ARM/SIRM ratio; however, also χ and SIRM would decrease, which contradicts the observed data. We may speculate that the highly variable and partly decreasing ARM/SIRM ratios in the Deccan basalts arise from competing effects of physical grain size and internal stress distribution, as suggested by Dunlop (2002). The large variability of experimental values reported for a given physical grain size (Maher, 1988) supports this assumption.

4.2. Climate-Related Variations

We assembled the bulk magnetic results as a function of MAP by both the slope values of linear regression (Figure 8) and the WP2/FR ratios (Figure 9). Both methods yield similar results as a function of MAP, with a few exceptions (notably χ and SIRM/χ of site DE33). The S-ratio and χ_{fd}% results are insignificant, as mentioned above, and we do not consider them for further discussion.

We generally notice only relatively small changes in the bulk magnetic properties, which is a good message for paleomagnetic studies. Magnetite in solid rock as collected by paleomagnetic sampling is likely not

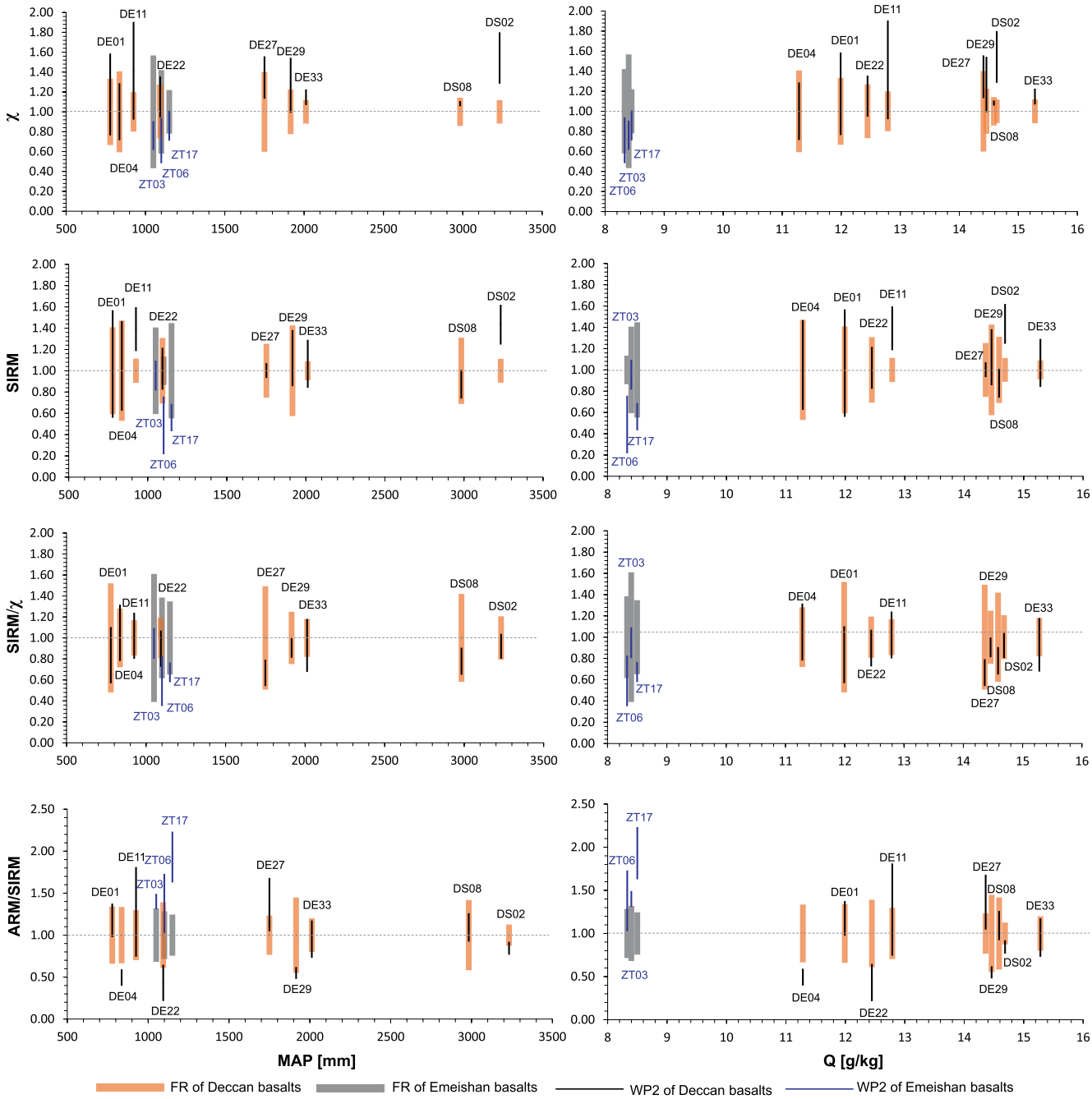

Figure 9. Ratio of WP2/FR parameter values versus mean annual precipitation (MAP; left column) and mean annual specific humidity (Q; right column), for χ (magnetic susceptibility), SIRM (saturation isothermal remanent magnetization), and ratios of SIRM/χ and ARM/SIRM (ARM: anhysteretic remanent magnetization). Thick bars (orange & gray: Deccan & Emeishan) show $\pm\sigma$ ranges (σ: standard deviation) of FR samples ($N = 5$) normalized to the corresponding mean value (mean = 1). Thin bars (black and blue: Deccan & Emeishan) show $\pm\sigma$ ranges of WP2 samples ($N = 5$) normalized to the mean of the corresponding FR samples. See Table S2 for numerical results. To avoid overlapping data in the plot, MAP-values for ZT03 (−50 mm) and ZT17 (+50 mm), and Q-values for ZT17 (+0.05 g/kg), DE27 (−0.05 g/kg), and DS02 (+0.05 g/kg) are slightly shifted.

changed to a degree of alteration that significantly disturbs the primary nature of magnetic remanences, possibly even not in weathered reddish-yellowish material as in the marginal part of the drill-core shown in Figure 1d.

Do the observed bulk properties show any systematic variation as function of MAP or MAT? Extracting a meaningful relationship with MAP is hindered by the relatively small effects of alteration. The χ-values increase with weathering for most Deccan sites as revealed by WP2/FR-ratios > 1 (1.234 ± 0.171). Linear regression analysis based on climate-data.org suggests that the increase of χ intensifies with higher MAP (0.013·MAP – 0.019 for slopes; 0.065·MAP + 1.123 for WP2/FR-ratios; MAP in [mm]). The trend is similar using ERA5 data (0.007·MAP – 0.011 for slopes; 0.104·MAP + 1.040 for WP2/FR-ratios). However, internal consistency of these data is limited (Figure 5), and the tendency of intensification with MAP is statistically insignificant. All other parameters and ratios from the Deccan sites do not reveal systematic changes with MAP. According to our modeling results (Figure 7), the increase of bulk χ values for the Deccan samples could be explained by progressive maghemitization, which enhances particle-internal subdivision and shifts part of the magnetite fraction into the SP range.

Additionally, to MAP, we analyzed the relationship of χ-changes and mean annual specific humidity (Q) (Figure 9). Specific humidity represents the amount of water vapor in the atmosphere as a result of precipitation and evaporation, and may better reflect the available moisture for magnetite alteration during rock weathering. Q-data are only available from ERA5. For WP2/FR-ratios ($0.045 \cdot Q + 0.623$) the trend of χ-values versus Q (in [g/kg]) principally agree with the trend versus MAP, but it is opposite for slope data ($-0.013 \cdot Q + 0.173$). Whether this indicates that the WP2/FR-ratio is more meaningful for reflecting magnetite alteration is unclear.

In contrast, a consistent change is observed for the three Emeishan (ZT) sites. Results of these sites show a decrease of magnetic concentration-dependent parameters (χ and SIRM) with progressive weathering (i.e., fining of WP fractions), a decreasing SIRM/χ ratio and an increasing ARM/SIRM ratio (Figures 8 and 9). The observed changes are at least partly distinguished within 95% confidence limits (Figure 8) and standard deviations (Figure 9) from zero change and from values of those Deccan sites with similar MAP values (~1,000 mm; DE01, DE04, DE11, and DE22). Indication for a systematic influence of MAT is therefore provided, with surprisingly a larger degree of alteration for the ~12°C–15°C lower MAT of the ZT samples. The possible role of the lower atmospheric water vapor content (Q) due to lower MAT is an open question. The significant decrease of the observed χ and SIRM values (Figures 8 and 9), consistent with the modeling results for D-2 (Figure 7), indicates that alteration of the weathered samples from the ZT sites includes the transformation of magnetite into a weakly magnetic phase (possibly hematite or goethite).

4.3. Were Sites and Samples Appropriate?

The Deccan basalts are certainly an appropriate target regarding a uniform type of rock across a large gradient of MAP, for allowing statistical analysis of large sample sets and supporting the magnetic results by meaningful microscopy observations. Uniformity of rock magnetic properties of the parent rock is a fundamental prerequisite for the study, and this concerns the question of whether the ferrimagnetic content actually consists of magnetite with no significant content of Ti-rich titanomagnetite.

The interpretation of the frequently observed hump in χ-T curves at intermediate temperatures played a crucial role for site selection. In principle, Ti-rich titanomagnetites may cause a hump-like shape by their temperature variation of χ (Appel & Soffel, 1985). At higher temperatures, the titanomagnetites will convert to magnetite and this conversion is revealed in χ-T heating curves (curve no. 3 in Figure 2e), an indication we used for rejecting sites. Moreover, part of the selected sites (DE04, DE11, DS08, and ZT03) do not show a hump (or only show a very small one) in the heating curve of the fresh rock samples, whereas a significant hump appears for samples from the weathered pebble fractions (Figure 3). Because of the metastability of Ti-rich titanomagnetites at normal temperature, new formation of Ti-rich titanomagnetites during weathering is impossible, and the trend toward developing or enhancing a hump for weathered pebbles excludes their presence. A hump may also be caused (partly or fully) by conversion of thermally instable maghemite (Deng et al., 2004; Dunlop & Özdemir, 1997; Kontny & Grothaus, 2017), however, this is irrelevant for the study as it implies that the humps in the studied basalts represent maghemitized magnetite.

Possible content of maghemitized magnetite in the original rock complicates the interpretation of the results in terms of alteration processes. The observed T_c values in fresh rock samples of up to ~50°C higher than expected for stoichiometric magnetite (580°C) might reflect pre-existing maghemitization in the parent rocks, as reported for synthetic (Özdemir & Banerjee, 1984) and natural samples (Gehring et al., 2009; Nishitani & Kono, 1983). In Figure 3, we notice more pronounced tails toward higher temperatures for fresh rock compared to pebble fractions, although a clear systematic trend is not indicated. Two processes might occur during weathering, that is, a loss of strongly maghemitized portions through mineral conversion (reducing the tail in χ-T curves) and an increase of progressively maghemitized portions (enhancing the tail in χ-T curves). The χ-T results (Figure 3) suggest that both processes are differently mixed, as we likewise discussed in Section 4.1 regarding the ARM/SIRM ratio. Conversion of maghemite could decrease the portion that shows relatively finer particle behavior, while variable maghemitization likely increases it, and the systematic trend in the hump intensity as a function of weathering will also be distorted. Eventually, neither the intensity of the hump nor the T_c-variation will provide suitable information on climate-dependent alteration of magnetite during rock weathering. This is likewise the case for the Verwey transition (VT), which is absent above a rather small degree of maghemizitation (Aragón et al., 1985). While the VT is detected with variable distinctness in the low-temperature χ-T curves of many fresh rock samples, indicating the existence of a mixture of (nesr-)stoichiometric and maghemitized magnetite in the parent rocks, it appears only in very few weathered pebble samples (Figure 3).

The variable appearance of the magnetite in the basalt samples, that is, different sizes and shapes of the magnetite-bearing grains and of magnetite in exsolution structures as well as internal subdivision of the magnetite, likely cause a strong difference for climate-related alteration. The FORC results (Figure 3) support a larger rock-type dependent difference compared to changes between fresh rock and weathered pebbles. Because of the rock-dependent heterogeneities and the small samples used in these measurements, statistical analysis of a huge amount of FORCs would be required to potentially identify systematic trends.

Grain size and lamellar texture as revealed in the micrographs (Figure 4) might allow to group the sites by their initial rock-type properties. However, the relationships of bulk magnetic parameters with MAP do not become more systematic when DE27 (very small magnetite-bearing grains) or DE27 and DE33 (no clear lamellar structures) are excluded. To which extent texture and grain size of the magnetite fraction influence the weathering-induced alteration eventually remains unclear.

4.4. Implication for Interpretation of Magnetic Proxies in Paleoclimatic Archives

Previous studies argued for a shift of magnetite properties in the Deccan Trap basalts from the MD state to the SSD and SP range through seasonal wetting in the monsoon months and oxidation of magnetite to hematite in hot-dry summers (Basavaiah, 2011; Khadkikar & Basavaiah, 2004). Laboratory experiments of Q. Zhang et al. (2021) demonstrated significant magnetite alteration due to humidity, with the strongest changes for persistently high humidity. Zhang et al. also reported a non-linear relationship of magnetic changes with humidity, and their results surprisingly indicated that alteration is relatively uniform across the entire particle volume, apart from possibly existing higher oxidized thin surface layers. The actualistic study of the Deccan basalts revealed only weakly consistent signals of humidity-related magnetite alteration.

The only weakly expressed (by χ) and mostly lacking (all other parameters) relationships with climate parameters (MAP or Q) are likely due to rock magnetic variability, that is, size and shape-specific characteristics of magnetite-bearing grains, and initial maghemitization of magnetite in the parent rock. Variability of rocks and rock-magnetic mineralogy obviously outweighs climate effects on magnetite alteration during rock weathering. Samples from five different sub-locations of the same site, and even samples within a single sub-locations, show high variability of rock magnetic properties (see single data points in Figures 5, 6 and S1–S4). This variability on spatial scales $<10^2$–10^3 m^2 (typical areas of sampled sites) will strongly influence rock magnetic properties of a sediment mixture derived from a catchment that in principle represents the same MAP.

We have analyzed the relationship of magnetic parameters as a function of annual means of precipitation and specific humidity, which are most likely the best indicators of average water or water vapor availability for magnetite alteration during rock weathering. We have not considered seasonal variations of climate

conditions (MAP, MAT, and Q) or high and low peak values. They may be an important driver of mineral alteration, but unfortunately, we have no access to such effects as proxy parameters, as magnetic properties of the weathered basalt materials, represent the product on a scale of long-term averaging. Nevertheless, the results of this study clearly indicate that among all possible other influencing processes (pedogenic, transport-related, and authigenic), humidity-dependent magnetite alteration during rock weathering can be excluded as a source of paleoclimate signals in the magnetic record of sedimentary archives (such as lake sediments) derived from weathered rocks in the catchment. Although humidity-related magnetite alteration likely exists, these effects are hidden by the magnetic variability in the source rocks. Because of rock magnetic variability on a small scale, changes in the mixture of transported sediment due to re-organization of water or wind transport pathways will easily wipe out systematic climate-related magnetite alteration that likely exists at small scale. The additional presence of Ti-rich titanomagnetites in the source rocks, which is common in many basalts, will even enhance the importance of the initial rock magnetic properties for the magnetic parameters of the weathered material.

In the strict sense, this study is valid if basalts occur in the catchment, dominating the magnetic properties of weathered material. In settings where no basalts occur in the catchment, the magnetic fraction in sedimentary archives may derive from weathered rocks with low magnetic variability of the parent rock. For large catchments, absence of any basaltic source materials is unlikely. The magnetic proxy signal in the ~940 m long sequence of the SG-1 core in the huge Qaidam Basin (NE Tibetan Plateau) was largely explained by maghemitization and magnetite-to-hematite transformation (Herb et al., 2013). In the light of the Deccan study, this interpretation should be reconsidered. In smaller catchments, a basaltic source rock may be absent. For example, the magnetic proxy signal in the lacustrine sequence of Heqing Basin (SE Tibetan Plateau) was explained by alteration of magnetite inherited from weathered limestones (Hu et al., 2015). However, the original source of detrital magnetite particles embedded in the weathered rock is unknown, as it often is the case in such settings, and therefore the problem arising from initial source rock variability might still exist, for the Heqing Basin and elsewhere in similar settings.

Relatively consistent results from the Emeishan basalts suggest a temperature-dependent effect of magnetite alteration, with stronger alteration than observed for the Deccan basalts, including both maghemitization and magnetite transformation (to hematite or goethite). The higher degree of alteration is surprising as the Emeishan sites are located in areas with ~12–15°C lower MAT than at the Deccan sites. The speed of chemical reactions generally decreases at lower temperatures. To explain this observation, we speculate on the effect of freezing and thawing, which occurs in the Emeishan sampling region in the winter seasons. Temperature cycling around the freezing point could lead to the formation of micro-cracks and nano-cracks, opening pathways for humidity and oxygen into the interior of the rock and magnetite-bearing grains.

5. Conclusions

Humidity-related alteration of magnetite, as suggested by previous laboratory studies, is slightly indicated by the results for parent rock weathering of the studied Deccan basalts, with an increasing degree of maghemitization for higher MAP. However, this trend is only very weakly supported at the statistical level.

A consistent effect of magnetite alteration is found for the Emeishan basalts. The alteration includes conversion of magnetite (likely to hematite or goethite). Surprisingly, the degree of alteration is stronger than for the Deccan basalts at similar MAP of ~1,100 mm, despite the ~12°C–15°C lower MAT. We hypothesize that this effect is caused by micro-cracks formed through freezing and thawing, opening pathways for humidity and oxygen into particle interiors.

High spatial variability of weathering-related magnetic properties is typical at the scale of the studied sites (i.e., areas $<10^2$–10^3 m^2). A shift in the mixing proportions of weathered materials from different locations within relatively small spatial extent might already lead to significant changes of rock magnetic properties in sediment sinks that are derived from these materials. As a consequence, climate-related magnetite alteration acquired during rock weathering is likely irrelevant for interpreting proxy records in paleoclimate archives such as lake sediments, at least for catchments with basaltic source rocks.

In further studies, other types of rock such as granites could be investigated, which may have better compositional homogeneity within and between samples.

Data Availability Statement

For climate data support, the authors thank ICDC, CEN, University of Hamburg. Data presented in this study are listed in the Supporting Information S1 and are available on Mendeley for public download at http://dx.doi.org/10.17632/x4hypc3gyd.1.

Acknowledgments
This study was supported by the German Research Foundation (DFG; AP 34/44-1), the National Natural Science Foundation of China (No. 41572152), and the Chinese Academy of Sciences Visiting Professorship for Senior International Scientists (Nos. 2012T1Z0004, 131432WGZJTPYJY2015002). Qi Zhang was the lead scientist in all parts of this study, Erwin Appel contributed to data analysis, interpretation and paper writing, Xiuhua Zhu processed the climate reanalysis data, Udo Neumann guided the microscopy analysis and interpretation, Nathani Basavaiah and Shouyun Hu organized the field campaigns and contributed to interpretations. The authors thank Tatiana Miranda for her support in SEM studies, Per Jeisecke and Simone Schafflick for embedding and polishing basalts sections. Open access funding enabled and organized by Projekt DEAL.

References

Abrajevitch, A., & Kodama, K. (2009). Biochemical vs. detrital mechanism of remanence acquisition in marine carbonates: A lesson from the K-T boundary interval. *Earth and Planetary Science Letters*, *286*, 269–277. https://doi.org/10.1016/j.epsl.2009.06.035

Allegre, C. J., Birck, J. L., Capmas, F., & Courtillot, V. (1999). Age of the Deccan traps using 187Re–187Os systematics. *Earth and Planetary Science Letters*, *170*(3), 197–204. https://doi.org/10.1016/S0012-821X(99)00110-7

Appel, E. (1987). Stress anisotropy in Ti-rich titanomagnetites. *Physics of the Earth and Planetary Interiors*, *46*, 233–240. https://doi.org/10.1016/0031-9201(87)90185-3

Appel, E., & Soffel, H. C. (1985). Domain state of Ti-rich titanomagnetites deduced from domain structure observations and susceptibility measurements. *Journal of Geophysics*, *56*, 121–132. https://geophysicsjournal.com/article/212

Aragón, R., Buttrey, D., Shepherd, J. P., & Honig, J. M. (1985). Influence of nonstoichiometry on the Verwey transition. *Physical Review B: Condensed Matter*, *31*, 436–436. https://doi.org/10.1103/PhysRevB.31.430

Basavaiah, N. (2011). Experimental geomagnetism. *Geomagnetism: Solid Earth and upper atmosphere perspectives*. Netherlands: Springer. https://doi.org/10.1007/978-94-007-0403-9_7

Basavaiah, N., Mahesh Babu, J. L. V., Gawali, P. B., Naga Kumar, K. C. V., Demudu, G., Prizomwala, S. P., et al. (2015). Late Quaternary environmental and sea level changes from Kolleru Lake, SE India: Inferences from mineral magnetic, geochemical and textural analyses. *Quaternary International*, *371*, 197–208. https://doi.org/10.1016/j.quaint.2014.12.018

Basavaiah, N., Satyanarayana, K. V. V., Deenadayalan, K., & Prasa, J. N. (2018). Does Deccan Volcanic Sequence contain more reversals than the three-Chron N–R–N flow magnetostratigraphy? A palaeomagnetic evidence from the dyke-swarm near Mumbai. *Geophysical Journal International*, *213*, 1503–1523. https://doi.org/10.1093/gji/ggy041

Bastian, L., Revel, M., BayonDufour, G. A., Vigier, N., & Vigier, N. (2017). Abrupt response of chemical weathering to Late Quaternary hydroclimate changes in northeast Africa. *Scientific Reports*, *7*, 44231. https://doi.org/10.1038/srep44231

Bloemendal, J., King, J. W., Hall, F. R., & Doh, S. J. (1992). Rock magnetism of Late Neogene and Pleistocene deep-sea sediments: Relationship to sediment source, diagenetic processes, and sediment lithology. *Journal of Geophysical Research: Solid Earth*, *97*(B4), 4361–4375. https://doi.org/10.1029/91JB03068

Bozorth, R. M. (1951). Magnetic domain patterns. *Journal de Physique et le Radium*, *12*(3), 308–321. https://doi.org/10.1051/jphysrad:01951001203030800

Cui, Y., Verosub, K. L., & Roberts, A. (1994). The effect of low-temperature oxidation on large multi-domain magnetite. *Geophysical Research Letters*, *21*(9), 757–760. https://doi.org/10.1029/94GL00639

Dearing, J. A., Dann, R. J. L., Hay, K., Lees, J., Loveland, P. J., Maher, B. A., & O'Grady, K. (1996). Frequency-dependent susceptibility measurements of environmental materials. *Geophysical Journal International*, *124*, 228–240. https://doi.org/10.1111/j.1365-246X.1996.tb06366.x

Dee, D. P., Uppala, S. M., Simmons, A. J., Berrisford, P., Poli, P., Kobayashi, S., et al. (2011). The ERA-Interim reanalysis: Conguration and performance of the data assimilation system. *Quarterly Journal of the Royal Meteorological Society*, *137*, 553–597. https://doi.org/10.1002/qj.828

Demory, F., Oberhansli, H., Nowaczyk, N. R., Gottschalk, M., Wirth, R., & Naumann, R. (2005). Detrital input and early diagenesis in sediments from Lake Baikal revealed by rock magnetism. *Global and Planetary Change*, *46*(1–4), 145–166. https://doi.org/10.1016/j.gloplacha.2004.11.010

Deng, C. L., Zhu, R. X., Verosub, K. L., Singer, M. J., & Vidic, N. J. (2004). Mineral magnetic properties of loess//paleosol couplets of the central loess plateau of China over the last 1.2 Myr. *Journal of Geophysical Research*, *109*, B01103. https://doi.org/10.1029/2003JB002532

Dunlop, D. J. (2002). Theory and application of the Day plot (Mrs/Ms versus Hcr/Hc) 1. Theoretical curves and tests using titanomagnetite data. *Journal of Geophysical Research*, *107*(B3). https://doi.org/10.1029/2001JB000486

Dunlop, D. J., & Argyle, K. S. (1997). Thermoremanence, anhysteretic remanence and susceptibility of submicron magnetites: Nonlinear field dependence and variation with grain size. *Journal of Geophysical Research: Solid Earth*, *102*(B9), 20199–20210. https://doi.org/10.1029/97JB00957

Dunlop, D. J., & Özdemir, Ö. (1997). *Rockmagnetism: Fundamentals and frontiers* (p. 573). Cambridge University Press.

Edwards, D. P., Lim, F., James, R. H., Pearce, C. R., Scholes, J., Freckleton, R. P., & Beerling, D. J. (2017). Climate change mitigation: Potential benefits and pitfalls of enhanced rock weathering in tropical agriculture. *Biology Letters*, *13*(4), 20160715. https://doi.org/10.1098/rsbl.2016.0715

Eriksson, M. G., & Sandgren, P. (1999). Mineral magnetic analyses of sediment cores recording recent soil erosion history in central Tanzania. *Palaeogeography, Palaeoclimatology, Palaeoecology*, *152*, 365–383. https://doi.org/10.1016/S0031-0182(99)00043-7

Gehring, A. U., Fischer, H., Louvel, M., Kunze, K., & Weidler, P. G. (2009). High temperature stability of natural maghemite: A magnetic and spectroscopic study. *Geophysical Journal International*, *179*(3), 1361–1371. https://doi.org/10.1111/j.1365-246X.2009.04348.x

Gorski, C. A., & Scherer, M. M. (2010). Determination of nanoparticulate magnetite stoichiometry by Mössbauer spectroscopy, acidic dissolution, and powder X-ray diffraction: A critical review. *American Mineralogist*, *95*, 1017–1026. https://doi.org/10.2138/am.2010.3435

Harrison, R. J., & Feinberg, J. M. (2008). FORCinel: An improved algorithm for calculating first-order reversal curve distributions using locally weighted regression smoothing. *Geochemistry, Geophysics, Geosystems*, *9*, Q05016. https://doi.org/10.1029/2008GC001987

He, Y., & Traina, S. J. (2007). Transformation of magnetite to goethite under alkaline pH conditions. *Clay Minerals*, *42*, 13–19. https://doi.org/10.1180/claymin.2007.042.1.02

Herb, C., Zhang, W. L., Koutsodendris, A., Appel, E., Fang, X. M., & Pross, J. (2013). Environmental implications of the magnetic record in Pleistocene lacustrine sediments of the Qaidam Basin, NE Tibetan Plateau. *Quaternary International*, *313–314*, 218–229. https://doi.org/10.1016/j.quaint.2013.06.015

Hersbach, H., Bell, B., Berrisford, P., Hirahara, S., Horányi, A., Muñoz-Sabater, J., et al. (2020). The ERA5 global reanalysis. *Quarterly Journal of the Royal Meteorological Society*, *146*, 1999–2049. https://doi.org/10.1002/qj.3803

Hu, S. Y., Goddu, S. R., Herb, C., Appel, E., Gleixner, G., Wang, S. M., et al. (2015). Climate variability and its magnetic response recorded in a lacustrine sequence in Heqing basin at the SE Tibetan Plateau since 900 ka. *Geophysical Journal International*, *201*, 444–458. https://doi.org/10.1093/gji/ggv033

Irving, E. (1970). The Mid-Atlantic Ridge at 45°N, XIV, Oxidation and magnetic properties of basalts: Review and discussion. *Canadian Journal of Earth Sciences*, *7*, 1528–1538. https://doi.org/10.1139/e70-144

Keller, R., & Schmidbauer, E. (1999). Magnetic hysteresis properties and rotational hysteresis losses synthetic stress-controlled titanomagnetite ($Fe_{2.4}Ti_{0.6}O_4$) particles - I. Magnetic hysteresis properties. *Geophysical Journal International*, *138*, 319–333. https://doi.org/10.1046/j.1365-246X.1999.00852.x

Khadkikar, A. S., & Basavaiah, N. (2004). Morphology mineralogy and magnetic susceptibility of epikarst-Terra Rossa developed in Late Quaternary aeolianite deposits of southeastern Saurashtra, India. *Geomormhology*, *58*, 339–355. https://doi.org/10.1016/j.geomorph.2003.07.001

Kodama, K. (2013). Application of broadband alternating current magnetic susceptibility to the characterization of magnetic nanoparticles in natural materials. *Journal of Geophysical Research: Solid Earth*, *118*, 1–12. https//doi.org/10.1029/2012JB009502

Kontny, A., & Grothaus, L. (2017). Effects of shock pressure and temperature on titanomagnetite from ICDP cores and target rocks of the El'gygytgyn impact structure, Russia. *Studia Geophysica et Geodaetica*, *61*, 162–183. https://doi.org/10.1007/s11200-016-0819-3

Lise-Pronovost, A., St-Onge, G., Gogorza, C., Jouve, G., Francus, P., Zolitschka, B., & PASADO Science Team. (2014). Rock-magnetic signature of precipitation and extreme runoff events in southeastern Patagonia since 51,200 cal BP from the sediments of Laguna Potrok Aike. *Quaternary Science Reviews*, *98*, 110–125. https://doi.org/10.1016/j.quascirev.2014.05.029

Liu, Q. S., Banerjee, S. K., Jackson, M. J., Chen, F., Pan, Y. X., & Zhu, R. X. (2004). Determining the climatic boundary between the Chinese loess and palaeosol: Evidence from aeolian coarse-grained magnetite. *Geophysical Journal International*, *156*(2), 267–274. https://doi.org/10.1111/j.1365-246X.2003.02148.x

Long, X. Y., Ji, J. F., & Balsam, W. (2011). Rainfall-dependent transformations of iron oxides in a tropical saprolite transect of Hainan Island, South China: Spectral and magnetic measurements. *Journal of Geophysical Research*, *116*, F03015. https://doi.org/10.1029/2010JF001712

Maher, B. A. (1988). Magnetic properties of some synthetic sub-micron magnetites. *Geophysical Journal International*, *94*(1), 83–96. https://doi.org/10.1111/j.1365-246X.1988.tb03429.x

Maher, B. A., & Hu, M. (2006). A high-resolution record of Holocene rainfall variations from the western Chinese Loess Plateau: Antiphase behaviour of the African/Indian and East Asian summer monsoons. *The Holocene*, *16*(3), 309–319. https://doi.org/10.1191/0959683606hl929rp

Maxbauer, D. P., Feinberg, J. M., Fox, D. L., & Clyde, W. C. (2016). Magnetic minerals as recorders of weathering, diagenesis, and paleoclimate: A core–outcrop comparison of Paleocene–Eocene paleosols in the Bighorn Basin, WY, USA. *Earth and Planetary Science Letters*, *452*, 15–26. https://doi.org/10.1016/j.epsl.2016.07.029

Mollo, S., Putirka, K., Iezzi, G., & Scarlato, P. (2013). The control of cooling rate on titanomagnetite composition: Implications for a geospeedometry model applicable to alkaline rocks from Mt. Etna volcano. *Contributions to Mineralogy and Petrology*, *165*, 457–475. https://doi.org/10.1007/s00410-012-0817-6

Mücke, A. (2003). Magnetite, ilmenite and ulvite in rocks and ore deposits: Petrography, microprobe analyses and genetic implications. *Mineralogy and Petrology*, *77*, 215–234. https://doi.org/10.1007/s00710-002-0216-1

Negrini, R. M., Erbes, D. B., Faber, K., Herrera, A. M., Roberts, A. P., Cohen, A. S., et al. (2000). A paleoclimate record for the past 250,000 years from Summer Lake, Oregon, USA: I. Chronology and magnetic proxies for lake level. *Journal of Paleolimnology*, *24*, 125–149. https://doi.org/10.1023/A:1008144025492

Nishitani, T., & Kono, M. (1983). Curie temperature and lattice constant of oxidized titanomagnetite. *Geophysical Journal International*, *74*, 585–586. https://doi.org/10.1111/j.1365-246X.1983.tb01890.x

O'Reilly, W. (1984). *Rock and mineral magnetism* (p. 220). Blackie London.

Özdemir, Ö., & Banerjee, S. K. (1984). High temperature stability of maghemite (γ-Fe2O3). *Geophysical Research Letters*, *11*(3), 161–164. https://doi.org/10.1029/GL011i003p00161

Özdemir, Ö., & Dunlop, D. J. (2010). Hallmarks of maghemitization in low-temperature remanence cycling of partially oxidized magnetite nanoparticles. *Journal of Geophysical Research*, *115*, B02101. https://doi.org/10.1029/2009JB006756

Peck, J. A., King, J. W., Colman, S. M., & Kravchinsky, V. A. (1994). A rock magnetic record from Lake Baikal, Siberia: Evidence for Late Quaternary climatic change. *Earth and Planetary Science Letters*, *122*, 221–238. https://doi.org/10.1016/0012-821X(94)90062-0

Petersen, N., & Vali, H. (1987). Observation of shrinkage cracks in ocean floor titanomagnetites. *Physics of the Earth and Planetary Interiors*, *46*, 197–205. https://doi.org/10.1016/0031-9201(87)90182-8

Radhakrishnamurty, C., Likhite, S. D., Deutsch, E. R., & Murthy, G. S. (1978). Nature of magnetic grains in basalts and implications for palaeomagnetism. *Proceedings of the Indian Academy of Sciences - Section A*, *87*, 235–243. https://doi.org/10.1007/BF02861518

Radhakrishnamurty, C., Likhite, S. D., & Sahasrabudhe, P. W. (1977). Nature of magnetic grains and their effect on the remanent magnetization of basalts. *Physics of the Earth and Planetary Interiors*, *13*(4), 289–300. https://doi.org/10.1016/0031-9201(77)90112-1

Radhakrishnamurty, C., & Sahasrabudhe, P. W. (1967). On the magnetic and mineralogical properties of basalts. *PAGEOPH*, *66*, 69–76. https://doi.org/10.1007/BF00875312

Ramdohr, P. (1980). *The ore minerals and their intergrowths* (2nd ed., p. 1207). Pergamon Press, University of California. ISBN 0080238017, 9780080238012.

Readman, P., & O'Reilly, W. (1972). Magnetic properties of oxidized (cation-deficient) titanomagnetites (Fe,Ti)3O_4. *Journal of Geomagnetism and Geoelectricity*, *24*, 69–90. https://doi.org/10.5636/jgg.24.69

Roberts, A. P., Heslop, D., Zhao, X. X., & Pike, C. R. (2014). Understanding fine magnetic particle systems through use of first-order reversal curve diagrams. *Reviews of Geophysics*, *52*, 557–602. https://doi.org/10.1002/2014RG000462

Schwertmann, U. (1985). The effect of pedogenic environments on iron oxide minerals. *Advances in Soil Sciences*, *1*, 171–200.

Shellnutt, J. G., & Jahn, B.-M. (2011). Origin of Late Permian Emeishan basaltic rocks from the Panxi region (SW China): Implications for the Ti-classification and spatial–compositional distribution of the Emeishan flood basalts. *Journal of Volcanology and Geothermal Research*, *199*, 85–95. https://doi.org/10.1016/j.jvolgeores.2010.10.009

Sheth, H. C. (2005). From Deccan to Réunion: No trace of a mantle plume. In G. R. Foulger, J. H. Natland, D. C. Presnall, & D. L. Anderson (Eds.), Plates, plumes, and paradigms (Vol. 388, pp. 477–501). Geological Society of America Special Papers. https://doi.org/10.1130/0-8137-2388-4.477

Sidhu, P. S. (1988). Transformation of trace element-substituted maghemite to hematite. *Clay Minerals*, *36*(1), 31–38. https://doi.org/10.1346/CCMN.1988.0360105

Snowball, I., Zillen, L., & Sandgren, P. (2002). Bacterial magnetite in Swedish varved lake sediments: A potential bio-marker of environmental change. *Quaternary International*, *88*, 13–19. https://doi.org/10.1016/S1040-6182(01)00069-6

Su, N., Yang, S. Y., Wang, X. D., Bi, L., & Yang, C. F. (2015). Magnetic parameters indicate the intensity of chemical weathering developed on igneous rocks in China. *Catena*, *133*, 328–341. https://doi.org/10.1016/j.catena.2015.06.003

Swaddle, T. W., & Oltmann, P. (1980). Kinetics of the magnetite–maghemite–hematite transformation, with special reference to hydrothermal systems. *Canadian Journal of Chemistry*, *58*(17), 1763–1772. https://doi.org/10.1139/v80-279

Torrent, J., Barron, V., & Liu, Q. (2006). Magnetic enhancement is linked to and precedes hematite formation in aerobic soil. *Geophysical Research Letters*, *33*, L02401. https://doi.org/10.1029/2005GL024818

Wang, D., Van der Voo, R., & Peacor, D. R. (2006). Low-temperature alteration and magnetic changes of variably altered pillow basalts. *Geophysical Journal International*, *164*, 25–35. https://doi.org/10.1111/j.1365-246X.2005.02819.x

Wensink, H. (1973). Newer paleomagnetic results of the Deccan traps, India. *Tectonophysics*, *17*(1–2), 41–59. https://doi.org/10.1016/0040-1951(73)90064-4

Worm, H. U. (1998). On the superparamagnetic-stable single domain transition for magnetite, and frequency dependence of susceptibility. *Geophysical Journal International*, *133*, 201–206. https://doi.org/10.1046/j.1365-246X.1998.1331468.x

Xu, Y. G., Chung, S. L., Jahn, B. M., & Wu, G. Y. (2001). Petrologic and geochemical constraints on the petrogenesis of Permian–Triassic Emeishan flood basalts in southwestern China. *Lithos*, *58*(3–4), 145–168. https://doi.org/10.1016/S0024-4937(01)00055-X

Yamazaki, T., & Ioka, N. (1997). Cautionary note on magnetic grain-size estimation using the ratio of ARM to magnetic susceptibility. *Geophysical Research Letters*, *24*(7), 751–754. https://doi.org/10.1029/97GL00602

Zhang, P., Lin, S., Ao, H., Wang, L. J., Sun, X. Y., & An, Z. S. (2016). Rock magnetism of the offshore sediments of Lake Qinghai in the Western China. *Frontiers of Earth Science*, *4*, 62. https://doi.org/10.3389/feart.2016.00062

Zhang, Q., Appel, E., Stanjek, H., Byrne, J. M., Berthold, C., Sorwat, J., et al. (2021). Humidity related magnetite alteration in an experimental setup. *Geophysical Journal International*, *224*, 69–85. https://doi.org/10.1093/gji/ggaa394